ACS APPLIED ELECTRONIC MATERIALS

pubs.acs.org/acsaelm Article

Effects of Excimer Laser Irradiation on the Morphological, Structural, and Electrical Properties of Aluminum-Implanted Silicon Carbide (4H-SiC)

Marilena Vivona,* Filippo Giannazzo, Gabriele Bellocchi, Salvatore Ethan Panasci, Simonpietro Agnello, Paolo Badalà, Anna Bassi, Corrado Bongiorno, Salvatore Di Franco, Simone Rascunà, and Fabrizio Roccaforte

Cite This: *ACS Appl. Electron. Mater.* 2022, 4, 4514–4520 Read Online

ACCESS | Metrics & More | Article Recommendations

ABSTRACT: This paper reports on the effects of excimer laser irradiation on an aluminum (Al)-doped silicon carbide (4H-SiC) layer. Specifically, high-concentration (1×10^{20} at/cm^3) Al-implanted 4H-SiC samples were exposed to a few pulses of 308 nm laser radiation (pulse duration of 160 ns), with fluence varying from 1.0 to 2.8 J/cm^2. As a starting point, the laser-induced modifications of the morphological, microstructural, and nano-electrical properties of the exposed 4H-SiC surface were monitored by combining different techniques. From these investigations, an evolution of the surface morphology was observed that can be ascribed to a conversion during irradiation of the uppermost part of the 4H-SiC implanted layer into a polycrystalline region of 3C-SiC and 6H-SiC grains, surmounted in the order by a crystalline-Si layer and an amorphous C-rich region. Then, the electrical characteristics of the implanted layer were evaluated by means of test structures appropriately fabricated on the samples. The high value of sheet-resistance of the irradiated layer (in the order of 10^4 kΩ/sq) suggested a poor activation of the p-type dopant and/or a low mobility of the carriers in the polycrystalline 3C-SiC/6H-SiC layer. The outcomes of this study can be useful for a fundamental understanding of laser annealing treatments of 4H-SiC implanted layers, toward a possible use in 4H-SiC technology of this process.

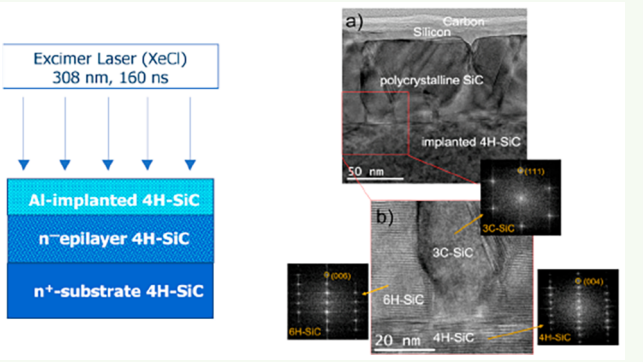

KEYWORDS: *silicon carbide (4H-SiC), laser annealing, Al-implantation, dopant activation*

INTRODUCTION

Nowadays, silicon carbide (4H-SiC) is the most established material for boosting progress in modern power electronics.[1] Specifically, this material offers outstanding physical properties, such as a wide bandgap (3.26 eV), high critical electrical field (>2 MV/cm) and high saturated drift velocity (>2 × 10^7 cm s^{-1}),[2] which enable huge performance improvements in high-power, high-temperature and high-frequency applications.[3] In spite of the successful employment of 4H-SiC-based Schottky diodes and metal-oxide-semiconductor field-effect transistors (MOSFETs) in several real applications (power supplies, AC/DC and DC/DC converters in automotive and industrial motors applications, DC/AC converters in photovoltaics, etc.),[3] some physical issues still need to be addressed for a further improvement of the device performances.[4]

Due to the low diffusivity of the dopant species in the material,[5] the ion-implantation technique is the consolidated method for selective doping in 4H-SiC power electronics devices, such as junction barrier Schottky (JBS) diodes or MOSFETs.[6,7] Nonetheless, the ion-implantation process inevitably leads to the production of lattice damage or even amorphization of the material.[8] Hence, postimplantation thermal annealing treatments are conventionally performed in furnaces at high temperature (>1600 °C),[9] to partially recover the crystalline structure of the semiconductor[10] and achieve the electrical activation of the dopant species, bringing them in substitutional lattice sites.[7] However, the electrical activation of the dopant species is limited by both their solid solubility and the attainable annealing temperature in conventional high temperature furnaces. Moreover, standard thermal annealing treatments at high temperatures can generate both

Received: June 7, 2022
Accepted: August 24, 2022
Published: September 1, 2022

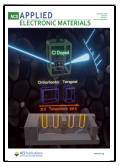

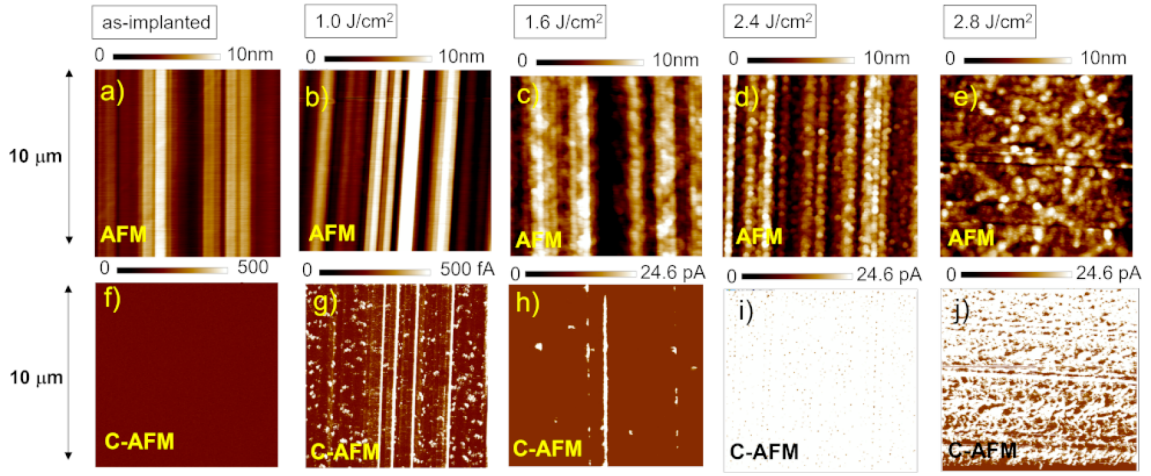

Figure 1. AFM micrographs (a–e) with the associated C-AFM current maps (f–j) on the surface of the 4H-SiC layer in the as-implanted case and in samples irradiated with four laser pulses of a XeCl laser with fluence varying from 1.0 to 2.8 J/cm^2. The four pulses have the same fluence.

point and extended defects, which are, in turn, detrimental for the electrical activation of the dopant.[11] Hence, a variety of unconventional nonequilibrium rapid thermal annealing processes have been explored to obtain high dopant incorporation avoiding the impurity deactivation due to solid solubility and defects.[12−15] Among them, pulsed-laser annealing methods can provide extremely fast heating ramps (in the order of 10^9 K/s) and allow us to locally reach much higher temperatures than conventional furnace annealing processes. Furthermore, these processes offer the advantage of a high localization and compatibility with wafer-scale processing. Finally, their employment can simplify 4H-SiC devices' fabrication, for instance by performing a patterned laser exposure of the implanted regions.

In recent years, most of the experimental and theoretical studies dealing with laser annealing treatments in 4H-SiC-technology have been focused to the formation mechanisms of back-side Ohmic contacts, with particular attention to nickel silicide.[16−22] However, less work has been reported on the effect of laser annealing directly on ion-implanted SiC layers. The earliest literature on this subject reported on the pulsed ultraviolet (UV) excimer laser annealing effects in 6H-SiC-implanted layers, with the aim of quantifying a possible dopant activation.[23−25] As an example, Ahmed et al. investigated the possible dopant activation produced by pulsed excimer laser exposure of N- and Al-implanted 6H-SiC, obtaining unrealistic activation levels (more than 100%) by means of point-contact current−voltage (PCIV) measurements, thus indicating the difficulty in the assessment of the dopant activation.[24] On the other hand, a quantitative evaluation of the electrical parameters of an irradiated (XeCl at 308 nm, 20 ns) P^+-implanted 4H-SiC layer was carried out by means of Hall measurements by Tanaka et al..[26] A sheet resistance R_{SH} value of 160 Ω/sq, comparable to that obtained after furnace annealing (1500 °C) of a similar implanted sample, was found only when the sample was kept at 800 °C under laser irradiation. However, four times lower mobility was observed in laser annealed sample if compared to the furnace-annealed one, which is explained with the presence of residual defects which act as scattering centers. For Al^+-ion-implanted 4H-SiC, Dutto et al.[14] found that a single-XeCl pulse 200 ns-long was sufficient to recover a large fraction of the implantation-induced defects and to achieve a partial dopant activation, as confirmed by I−V measurements on mesa p−n junction diodes. However, the observed high on-state resistance and poor forward conduction of the p-n diodes indicted the need of better in-depth analyses to elucidate the laser-induced effects on the Al-implanted 4H-SiC layer.

In this work, the effects of laser annealing treatment on Al-implanted 4H-SiC layers were monitored upon different 308 nm laser irradiation fluences. The combination of several techniques enabled explanation of the evolution of the morphological, microstructural and electrical properties of the laser-irradiated layers.

EXPERIMENTAL SECTION

The starting material of our investigation consists of an n-type 4H-SiC epitaxial layer with nominal doping concentration of about 1×10^{16} at/cm^3, grown on an n^+-doped (5×10^{18} at/cm^3) substrate. This layer was implanted with Al-ions at 500 °C using energies ranging between 30 and 200 keV and doses between 3×10^{14} and 1×10^{15} at/cm^2. From these implantation conditions, an almost flat profile with a thickness t_{impl} of about 300 nm and an Al-ion-implanted concentration up to about 1×10^{20} at/cm^3 was created. The sample surface was then irradiated by a UV pulsed excimer (XeCl) laser at 308 nm, pulse duration of 160 ns and frequency of 4 Hz, with fluences ranging between 1.0 and 2.8 J/cm^2. The laser beam was shaped by a homogenizer, which produced a uniform intensity on a 10 mm × 10 mm area.

The surface morphology was investigated by means of atomic force microscopy (AFM), using a Digital Instrument D3100 equipped with a Nanoscope V controller, in sample regions of 10 μm × 10 μm. The local electrical behavior was evaluated by conductive an AFM (C-AFM) technique, acquired by scanning a metal tip (connected to a current amplifier) on the same sample surface, while applying a potential difference between the tip and the sample back-side. The microstructural characteristics of the Al-implanted samples subjected to laser irradiation were studied by dark field scanning transmission electron microscopy (STEM) and transmission electron microscopy (TEM) techniques applied in cross section, using a 200 kV JEOL2010F microscope. The laser-induced structural changes were also monitored by means of a confocal Raman spectrometer (Horiba HR-Evolution microRaman system) equipped with a 100× objective. Spectra were excited at 532 nm, with a power of about 3 mW, dispersed by a 600 or 1800 grooves/mm grating and acquired by a charge-coupled device (CCD) camera.

In order to determine the electrical properties of the laser-irradiated Al-implanted layers, circular transmission line model (C-TLM)[27] structures were fabricated by optical lithography using a

https://doi.org/10.1021/acsaelm.2c00748
ACS Appl. Electron. Mater. 2022, 4, 4514−4520

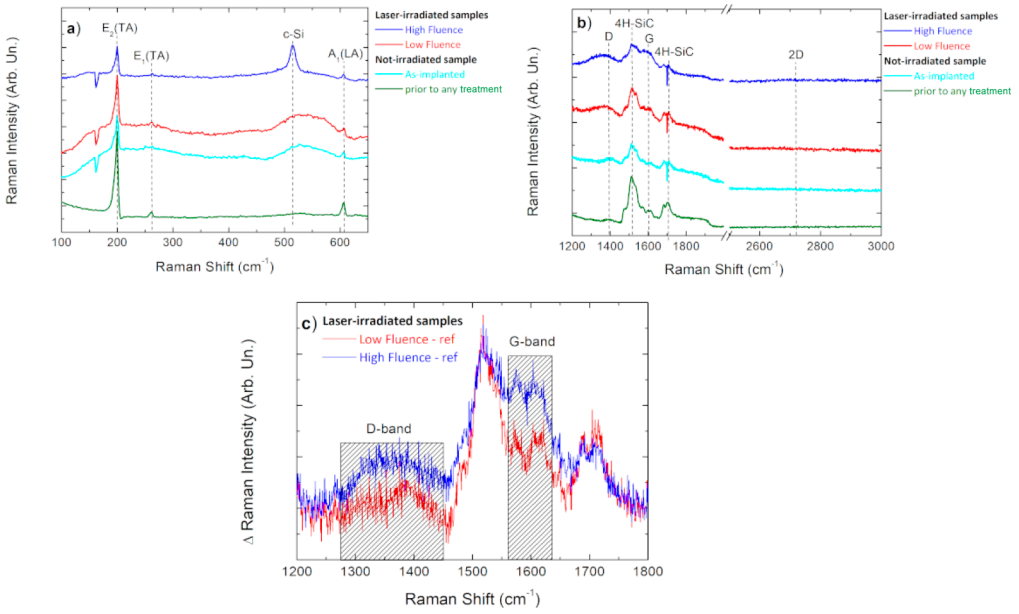

Figure 2. Raman spectra of the reference sample (4H-SiC layer prior any treatment, i.e., not-implanted and not-irradiated), an as-implanted sample, and two samples with Al-implanted 4H-SiC layers irradiated by laser at low (four pulses at 1.6 J/cm^2) and high fluence (four pulses at 2.4 J/cm^2) detected in the ranges (a) 100−650 cm^{-1} and (b) 1200−3000 cm^{-1}. *c)* Detailed Raman region related to C−C vibrations. Spectra were obtained by subtracting the Raman spectrum of the reference sample.

sequential sputter deposition of Ti (10 nm) and Ni (100 nm) layers and an annealing treatment at 950 °C in N_2 for 60 s. Specifically, the C-TLM structures had an inner radius of 200 μm and distances ranging from 20 to 40 μm. The current−voltage (I−V) measurements on the C-TLM structures were performed on a Karl Suss Microtec probe station with a HP 4156B parameter analyzer in a four-point probe configuration, with measurement temperature varying from 25 to 125 °C.

RESULTS AND DISCUSSION

Properties of the Exposed 4H-SiC Surface. First, we monitored the morphological and local current conduction properties of the 4H-SiC surface exposed to different laser irradiation fluences, from 1.0 to 2.8 J/cm^2. Figure 1 displays the morphological images acquired on the laser-irradiated samples, together with the corresponding C-AFM current maps. As a reference, in the same figure the morphology and current maps of an Al-implanted 4H-SiC layer not subjected to a laser irradiation process (labeled *as-implanted* sample) are reported.

The AFM images of the sample surface (Figure 1a−e) showed a clear evolution of the morphological features. In detail, starting by comparing Figure 1a and b, no significant modification of the pristine surface morphology, characterized by the presence of step bunching, was observed upon irradiation at 1.0 J/cm^2. However, following the irradiation at 1.6 J/cm^2, the pristine surface morphology changed, with the steps becoming smoother and the appearance of micrometer-size features overlapping the original steps. A gradual enhancement of this trend was observed with increasing the laser fluence, until these micrometer-size features entirely covered the sample surface (Figure 1e), with the root-mean-square (RMS) roughness decreasing from 3.51 to 2.17 nm. The local conduction investigation by the C-AFM technique revealed a low current level in the as-implanted sample. Following the laser exposure, the current level started to increase, as highlighted in the associated C-AFM shown in Figure 1g and h, up to a saturation condition visible for the 2.4 and 2.8 J/cm^2-irradiated samples (Figure 1i and j). This strong increase of the vertical injected current with increasing the laser fluence is correlated with the appearance of the micrometric-size features recovering the surface. The nature of this microstructural modification in the near-surface 4H-SiC region was highlighted by the following structural/chemical analyses based on Raman and TEM-analyses.

Raman spectroscopy was performed to provide an overall view on the laser-induced modifications of the 4H-SiC irradiated layers. Raman spectra were detected in two significant regions, as reported in Figure 2a and b. Specifically, for the 100−650 cm^{-1} region (Figure 2a), we observed in a sample prior to any treatment (a 4H-SiC layer neither implanted nor laser-irradiated) the presence of the 4H-SiC crystalline peaks E_2(TA), E_1(TA), and A_1(LA), centered at 198, 260, and 604 cm^{-1}, respectively. The same three signals were visible in the as-implanted sample, with in addition a broad background associated with an amorphization process of the 4H-SiC layer.[28,29] A band around 550 cm^{-1}, which can be ascribed to the amorphous Si−Si vibration,[30] appeared in the same sample. No variations of the Raman features occurred for a low-fluence (four pulses at 1.6 J/cm^2) irradiated sample, indicating a negligible effect of the laser treatment under this condition. Instead, a new Raman signal appeared in a higher-fluence (four pulses at 2.4 J/cm^2) irradiated sample, with a well-isolated peak at 520 cm^{-1}, associated with crystalline Si (c-Si) vibrations and the concurrent reduction of the band related to the amorphous Si vibration, peaked at 550 cm^{-1}. In addition, a reduction of the broad hump in the background was observed. Especially, the Raman characterization in the 1200−3000 cm^{-1} range is useful to highlight the disorder degree of the C-rich layers. As shown in Figure 2b, the spectrum of the sample prior to any treatments and the as-implanted one exhibited the characteristic second-order Raman peaks of the 4H-SiC at around 1518 and 1711 cm^{-1}.[31] For the laser-exposed samples, we observed the increase of the Raman

https://doi.org/10.1021/acsaelm.2c00748
ACS Appl. Electron. Mater. 2022, 4, 4514−4520

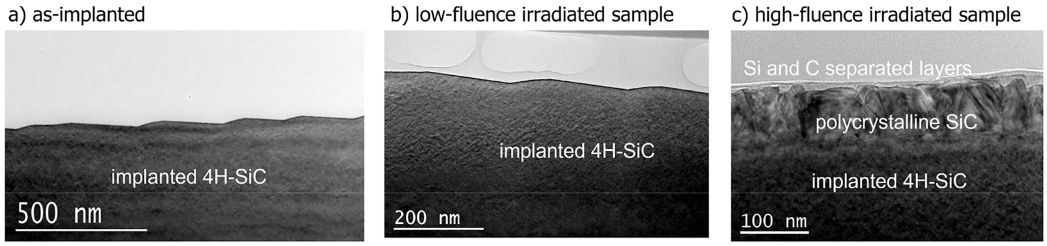

Figure 3. Cross-sectional TEM images of Al-implanted 4H-SiC layer (a) not exposed to laser irradiation (as-implanted), (b) irradiated at 1.4 J/cm^2, and (c) irradiated at 2.6 J/cm^2 with four pulses.

signals associated with C−C vibrations centered at 1361 cm^{-1}, which can be attributed to the defect-induced D-band, and the peak at 1584 cm^{-1} related to the G-band.[32] These features are reported in more detail in Figure 2c, with the other Raman peaks related to 4H-SiC contributions.[33] In particular, the absence of the doublet structure in the D-band and its second order 2D-band (2700−2750 cm^{-1}[32]) indicates the presence of an amorphous C region.[34]

In order to provide further insights on these aspects, the changes in the microstructural properties were studied by cross-sectional TEM analysis. In Figure 3, we compare the TEM images of three Al-implanted samples, consisting of the as-implanted sample and two samples irradiated with four pulses at 1.4 and 2.6 J/cm^2. Specifically, the low-fluence irradiated 4H-SiC layer, displayed in Figure 3b, does not show any significant modification with respect to the as-implanted sample (Figure 3a). In fact, in both samples, the terraces and facets of the steps were clearly visible in the surface, while a defective region produced by the ion-implantation can be clearly identified under the surface. It is important to note that, for the high value of implantation dose employed in our work, it is difficult to recover the crystal damage fully or partially with conventional or even relatively low-annealing-temperature treatments.[35] Instead, as one can see in Figure 3c, in the high-fluence irradiated sample a very different surface was observed, with an about 100 nm thick polycrystalline layer including 3C and 6H-SiC grains. In addition, two separated upper layers, consisting of a carbon-rich region and an underlying crystalline−silicon layer, were present on the top. This is visible in more detail in Figure 4.

The presence of this conductive carbon region on the surface is the main reason for the strong increase in the vertical injected current observed in the C-AFM maps reported in Figure 1i and l.

Specifically, focusing on the polycrystalline SiC layer, Figure 4a and b shows increasingly magnified TEM images of this part, detected in the same region of Figure 3c. The analysis of the diffraction patterns, observed along the [11-20] direction of the 4H-SiC layer for three indicative regions, reveals the coexistence of 3C-SiC and 6H-SiC grains, epitaxially grown on the 4H-SiC layer. In fact, thanks to this epitaxial alignment, the three phases (4H, 6H and 3C) are clearly recognized by diffraction patterns taken along the [11-20] direction of the SiC substrate. he phases can be unequivocally associated with the number of spots counted before the d = 0.25 nm reflection present in all the phases: three spots before the (004) reflection in 4H, two spots before the (006) reflection in 6H, and no spots before the (111) reflection in 3C. As a consequence, both the hexagonal phases showed fringes parallel to the surface in the high-resolution TEM images,

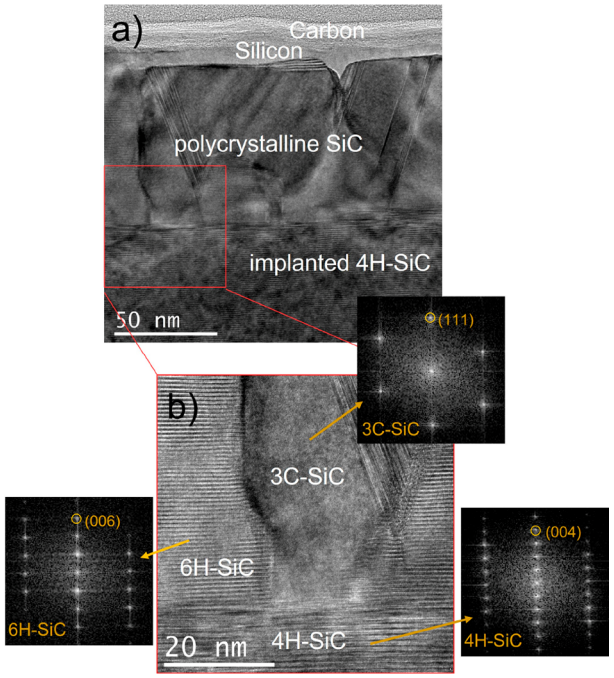

Figure 4. (a) TEM image of the surface layers in the sample irradiated at high fluence. (b) High-resolution image of the inset in part a. Fast Fourier transformation (FFT) patterns of the three phases are reported.

while the cubic phase did not show fringes but on the other side presented visible stacking fault defects.

Qualitatively, these results indicate that a melting of the implanted 4H-SiC layer and its recrystallization in two different polytypes occurred,[10,36] accompanied by a phase-separation of Si and C close to the sample surface. This process is induced by the energy supplied by the four pulses at 2.6 J/cm^2, thus resulting below the threshold for the Si-atom evaporation in this system.

An estimation of the temperature reached upon laser irradiation as a function of the distance x from the irradiated surface can be obtained by means of eq 1.[37] It is noteworthy that this relationship is valid in the thermal diffusion regime.

$$T(x) = \frac{I_0(1-R)}{K}\left[\sqrt{\frac{4D_T\tau}{\pi}}\, e^{-x^2/4D_T\tau} - x\,\mathrm{erfc}\left(\frac{x}{\sqrt{4D_T\tau}}\right)\right] + T_0 \quad (1)$$

with I_0 the laser irradiance (in W × m^{-2}), K the thermal conductivity of 4H-SiC (~370 W × m^{-1} × K^{-1}),[38] R the implanted 4H-SiC reflectivity (0.27),[39] D_T the thermal diffusivity (~1.7 × 10^{-4} m^2/s), τ the irradiation time (160 × 10^{-9} s), and T_0 the initial surface temperature (293 K).

https://doi.org/10.1021/acsaelm.2c00748
ACS Appl. Electron. Mater. 2022, 4, 4514−4520

Figure 5 reports the sample temperature as a function of the depth, calculated using eq 1 for various fluences (from 1.4 to 2.6 J/cm^2). The inset shows the temperature profiles in the first 500 nm from the surface, that is the region where the implantation profile is confined and thermal effects were mainly investigated.

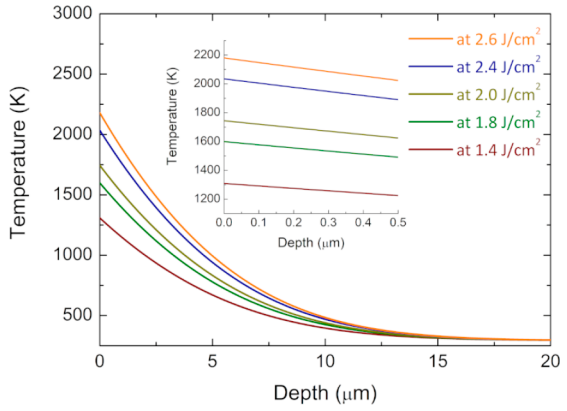

Figure 5. Simulated temperature profile as a function of the depth from the surface for pulse irradiation with fluence varying from 1.4 J/cm^2 to 2.6 J/cm^2. The inset shows the temperature profile in the first 500 nm.

Evidently, at the sample surface irradiated at low fluence (1.4 J/cm^2), a temperature of ∼1300 K is expected, while a temperature higher than 2100 K is reached in the high-fluence (2.6 J/cm^2) irradiated sample. As observed by TEM analysis, for this latter sample the laser exposure energy was sufficient for producing melting condition, in line with the occurrence of this phenomenon in noncrystalline 4H-SiC at temperatures below the melting temperature threshold (about 3100 K) for crystalline 4H-SiC.[40]

Electrical Properties of the 4H-SiC Implanted Layer. C-TLM test patterns fabricated using Ti/Ni contacts were used to evaluate the electrical properties of the 4H-SiC Al-implanted layer after laser irradiation. Electrical analysis was performed on three different samples irradiated with two pulses at 1.6 and 2.0 and at 2.4 J/cm^2. In order to get information on the electrical characteristics of the implanted layer, prior to the Ti/Ni-pad definition, the upper carbon-rich and c-Si layers were removed by means of an oxidation process at 800 °C, followed by a wet etching in diluted HF. Before fabricating the C-TLM test patterns, nondestructive C-AFM analyses were carried out on the sample surface, to check if the conductive carbon-rich and c-Si layers were effectively removed by the oxidation process. We investigated the electrical behavior in three different cases, i.e., for laser exposure at 1.6, 2.0 and 2.4 J/cm^2. A very low current conduction was detected for the 1.6 and 2.0 J/cm^2-irradiated 4H-SiC implanted layers, with I−V characteristics that did not show a dependence on the C-TLM pad distance. Therefore, the C-TLM method cannot supply any useful information on these two contacts. Instead, the sample irradiated at the highest fluence (2.4 J/cm^2) showed linear I−V characteristics, with a total resistance increasing with the pad distance. Hence, we focused our analysis on the sample irradiated at 2.4 J/cm^2.

Figure 6a shows the room-temperature I−V characteristics, acquired on the C-TLM patterns fabricated on this sample. The total resistance (R_{TOT}) values, determined by the slopes of the I−V curves, are reported in Figure 6b as a function of the pad distance. As can be seen, high values of R_{TOT} are measured, i.e., in the order of hundreds of kΩ.

According to the C-TLM method,[41] the sheet resistance R_{SH} of the layer was determined from the slope of the linear fit of R_{TOT} as a function of the pad distance. In particular, this analysis was applied to the I−V measurements acquired on the C-TLM structures at different temperatures varying from 298 to 398 K.

Figure 7a reports the values of R_{SH} for the laser-irradiated Al-implanted layer, as a function of the measurement temperature. The sheet resistance decreased from a value of $R_{SH} = (1.62 \pm 0.03) \times 10^4$ kΩ/sq extracted at room temperature down to $(3.18 \pm 0.06) \times 10^3$ kΩ/sq for the highest tested temperature. It is noteworthy that this trend with temperature is typically observed in doped semiconductors. In order to gain insight on the system, in Figure 7b we plot in an Arrhenius form the R_{SH} values of Figure 7a, obtaining an activation energy of about 166 meV. Considering that the Al-ions are embedded in a polycrystalline 3C-SiC/6H-SiC region, this value can be considered as an effective Al-ionization energy in this complex system.

From the values of the sheet resistance, assuming that the current flow occurs mainly in the 100 nm thick layer composed by 3C-SiC and 6H-SiC grains, observed by TEM analyses (Figure 4), it was possible to estimate a value of the resistivity of this layer $\rho = 160\ \Omega \times$ cm at room temperature. This value is significantly higher than the value of 0.36 Ω × cm measured

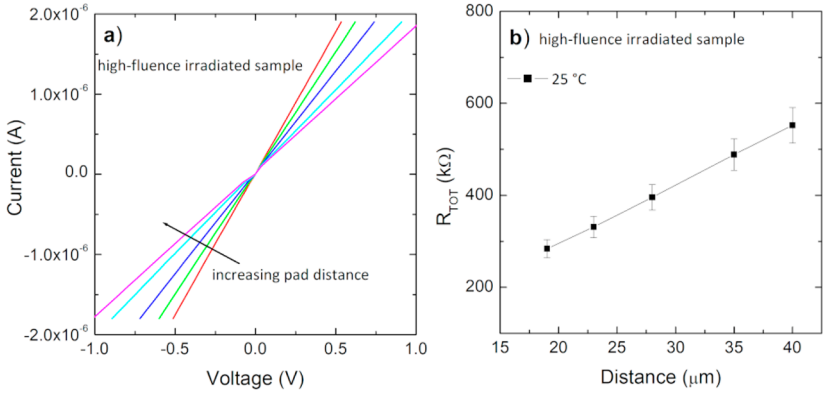

Figure 6. (a) Room-temperature I−V curves acquired on the C-TLM structures for different pad distances. (b) Related total resistance, extrapolated from the slope of the I−V curves for the different pad distances.

https://doi.org/10.1021/acsaelm.2c00748
ACS Appl. Electron. Mater. 2022, 4, 4514−4520

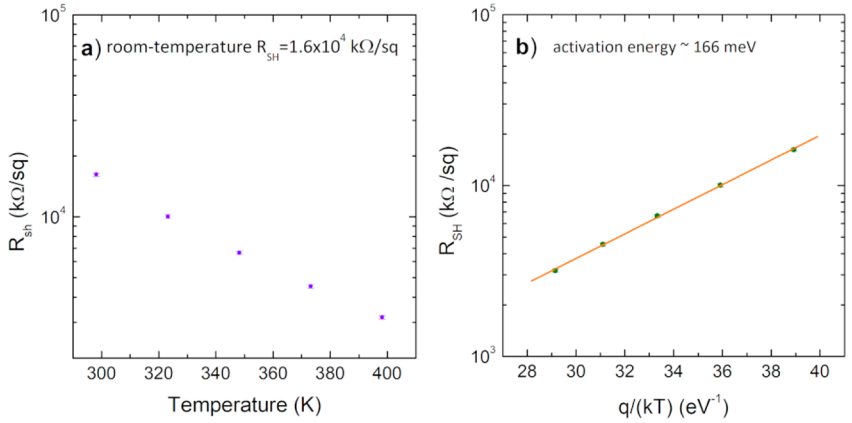

Figure 7. (a) Temperature-dependence of the sheet resistance R_{SH} . (b) Related Arrhenius' plot R_{SH} vs q/kT for deriving the activation energy.

in a 4H-SiC sample implanted under the same conditions and subjected to conventional thermal annealing at 1675 °C for the electrical activation.[42] Hence, it is reasonable that a very low electrical activation (<1%) of the Al-implanted species and/or a poor mobility of the carriers in the polycrystalline layer is obtained in this kind of system.

CONCLUSION

In this work, we have characterized Al-implanted 4H-SiC layers subjected to few pulses of 308 nm laser radiation. The effects of the laser irradiation for increasing fluences, varying from 1.0 to 2.8 J/cm^2, were studied by combining different techniques in order to highlight the morphological, microstructural and nanoelectrical modifications of the exposed 4H-SiC sample surface. An evolution of the surface morphology was observed with increasing the laser fluence, explained with the formation, from outside to inside, of an amorphous-C rich region, a crystalline Si-layer and a polycrystalline region with the presence of 3C and 6H-SiC grains upon a residual implanted 4H-SiC layer. The electrical analysis of the implanted layer showed a sheet resistance decreasing with increasing the measurement temperature, which resembles the behavior of a p-type doped material. However, the values of the resistivity were significantly higher than those obtained under a conventional annealing process, this indicating either a poor electrical activation or a low carrier mobility in the polycrystalline region formed after laser irradiation. The outcomes of this study can be useful for a fundamental understanding of the mechanisms involved in laser annealing treatments of a 4H-SiC-implanted layer and pave the way for the possible implementation in real device processing.

AUTHOR INFORMATION

Corresponding Author

Marilena Vivona − *Consiglio Nazionale delle Ricerche (CNR), Istituto per la Microelettronica e Microsistemi (IMM), I-95121 Catania, Italy;* orcid.org/0000-0002-0765-8556; Email: marilena.vivona@imm.cnr.it

Authors

Filippo Giannazzo − *Consiglio Nazionale delle Ricerche (CNR), Istituto per la Microelettronica e Microsistemi (IMM), I-95121 Catania, Italy;* orcid.org/0000-0002-0074-0469

Gabriele Bellocchi − *STMicroelectronics Stradale Primosole, I-95121 Catania, Italy*

Salvatore Ethan Panasci − *Consiglio Nazionale delle Ricerche (CNR), Istituto per la Microelettronica e Microsistemi (IMM), I-95121 Catania, Italy; Department of Physics and Astronomy, University of Catania, I-95123 Catania, Italy*

Simonpietro Agnello − *Consiglio Nazionale delle Ricerche (CNR), Istituto per la Microelettronica e Microsistemi (IMM), I-95121 Catania, Italy; Department of Physics and Chemistry Emilio Segrè, University of Palermo, I-90123 Palermo, Italy; ATEN Center, University of Palermo, I-90128 Palermo, Italy;* orcid.org/0000-0002-0346-8333

Paolo Badalà − *STMicroelectronics Stradale Primosole, I-95121 Catania, Italy*

Anna Bassi − *STMicroelectronics Stradale Primosole, I-95121 Catania, Italy*

Corrado Bongiorno − *Consiglio Nazionale delle Ricerche (CNR), Istituto per la Microelettronica e Microsistemi (IMM), I-95121 Catania, Italy*

Salvatore Di Franco − *Consiglio Nazionale delle Ricerche (CNR), Istituto per la Microelettronica e Microsistemi (IMM), I-95121 Catania, Italy*

Simone Rascunà − *STMicroelectronics Stradale Primosole, I-95121 Catania, Italy*

Fabrizio Roccaforte − *Consiglio Nazionale delle Ricerche (CNR), Istituto per la Microelettronica e Microsistemi (IMM), I-95121 Catania, Italy;* orcid.org/0000-0001-8632-0870

Complete contact information is available at: https://pubs.acs.org/10.1021/acsaelm.2c00748

Notes

The authors declare no competing financial interest.

ACKNOWLEDGMENTS

The authors would like to acknowledge G. Greco (CNR-IMM), P. Fiorenza (CNR-IMM), and M. Saggio (STMicroelectronics) for fruitful discussions. The data that support the findings of this study are available from the corresponding author upon reasonable request.

REFERENCES

(1) Kimoto, T. Material science and device physics in SiC technology for high-voltage power devices. *Jpn. J. Appl. Phys.* **2015**, *54*, 040103.

(2) Kimoto, T.; Cooper, J. A. *Fundamentals of Silicon Carbide Technology*; John Wiley & Sons Pte. Ltd.: Singapore, 2014.

(3) She, X.; Huang, A. Q.; Lucía, Ó.; Ozpineci, B. Review of Silicon Carbide Power Devices and Their Applications. *IEEE Transactions on Industrial Electronics* **2017**, *64*, 8193−8205.
(4) Roccaforte, F.; Fiorenza, P.; Greco, G.; Lo Nigro, R.; Giannazzo, F.; Iucolano, F.; Saggio, M. Emerging trends in wide band gap semiconductors (SiC and GaN) technology for power devices. *Microelectron. Eng.* **2018**, *187*−*188*, 66−77.
(5) Harris, G. L. Diffusion of impurities and ion implantation. In *Properties of Silicon Carbide*; Harris, G. L., Ed.; INSPEC, the Institution of Electrical Engineers: London, UK, 1995; pp 151−157.
(6) Hallén, A.; Linnarsson, M. Ion implantation technology for silicon carbide. *Surf. Coat. Technol.* **2016**, *306*, 190−193.
(7) Roccaforte, F.; Fiorenza, P.; Vivona, M.; Greco, G.; Giannazzo, F. Selective Doping in Silicon Carbide Power Devices. *Materials* **2021**, *14*, 3923.
(8) Svensson, B. G.; Hallén, A.; Linnarsson, M. K.; Kuznetsov, A. Y.; Janson, M. S.; Formanek, B.; Österman, J.; Persson, P. O.; Hultman, L.; Storasta, L.; Carlsson, F. H. C.; Bergman, P.; Jagadish, C.; Morvan, E. Doping of Silicon Carbide by Ion Implantation. *Mater. Sci. Forum* **2001**, *353*−*356*, 549−554.
(9) Kimoto, T.; Inoue, N. Nitrogen Ion Implantation into α-SiC Epitaxial Layers. *Phys. Stat. Sol. A* **1997**, *162*, 263−276.
(10) Hedler, A.; Urban, S.; Falk, F.; Hobert, H.; Wesch, W. Excimer laser crystallization of amorphous silicon carbide produced by ion implantation. *Appl. Surf. Sci.* **2003**, *205*, 240−248.
(11) Wendler, E.; Heft, A.; Wesch, W. Ion-beam induced damage and annealing behaviour in SiC. *Nucl. Instr. Meth. Phys. B* **1998**, *141*, 105−117.
(12) Sundaresan, S. G.; Rao, M. V.; Tian, Y.; Ridgway, M. C.; Schreifels, J. A.; Kopanski, J. J. Ultrahigh-temperature microwave annealing of Al^+- and P^+-implanted 4H-SiC. *J. Appl. Phys.* **2007**, *101*, 073708.
(13) Maruyama, K.; Hanafusa, H.; Ashihara, R.; Hayashi, S.; Murakami, H.; Higashi, S. High-efficiency impurity activation by precise control of cooling rate during atmospheric pressure thermal plasma jet annealing of 4H-SiC wafer. *Jpn. J. Appl. Phys.* **2015**, *54*, 06GC01.
(14) Dutto, C.; Fogarassy, E.; Mathiot, D.; Muller, D.; Kern, P.; Ballutaud, D. Long-pulse duration excimer laser annealing of Al^+ ion implanted 4H-SiC for pn junction formation. *Appl. Surf. Sci.* **2003**, *208*−*209*, 292−297.
(15) Tanaka, Y.; Tanoue, H.; Arai, K. Electrical activation of the ion-implanted phosphorus in 4H-SiC by excimer laser annealing. *J. Appl. Phys.* **2003**, *93*, 5934−5936.
(16) Berger, C.; Michaud, J.-F.; Chouteau, D.; Alquier, D. Laser Annealing Simulations of Metallisations Deposited on 4H-SiC. *Mater. Sci. Forum* **2019**, *963*, 502−505.
(17) De Silva, M.; Ishikawa, S.; Miyazaki, T.; Kikkawa, T.; Kuroki, S.-I. Formation of amorphous alloys on 4H-SiC with NbNi film using pulsed-laser annealing. *Appl. Phys. Lett.* **2016**, *109*, 012101.
(18) Mazzamuto, F.; Halty, S.; Tanimura, H.; Mori, Y. Low Thermal Budget Ohmic Contact Formation by Laser Anneal. *Mater. Sci. Forum* **2016**, *858*, 565−568.
(19) Badalà, P.; Rascunà, S.; Cafra, B.; Bassi, A.; Smecca, E.; Zimbone, M.; Bongiorno, C.; Calabretta, C.; La Via, F.; Roccaforte, F.; Saggio, M.; Franco, G.; Messina, A.; La Magna, A.; Alberti, A. Ni/4H-SiC interaction and silicide formation under excimer laser annealing for ohmic contact. *Materialia* **2020**, *9*, 100528.
(20) Rascunà, S.; Badalà, P.; Tringali, C.; Bongiorno, C.; Smecca, E.; Alberti, A.; Di Franco, S.; Giannazzo, F.; Greco, G.; Roccaforte, F.; Saggio, M. Morphological and electrical properties of Nickel based Ohmic contacts formed by laser annealing process on n-type 4H-SiC. *Mater. Sci. Semicond. Process.* **2019**, *97*, 62−66.
(21) Sanzaro, S.; Bongiorno, C.; Badalà, P.; Bassi, A.; Deretzis, I.; Enachescu, M.; Franco, G.; Fisicaro, G.; Vasquez, P.; Alberti, A.; La Magna, A. Simulations of the Ultra-Fast Kinetics in Ni-Si-C Ternary Systems under Laser Irradiation. *Materials* **2021**, *14*, 4769.
(22) Rupp, R.; Elpelt, R.; Gerlach, R.; Schomer, R.; Draghici, M. A. A new SiC diode with significantly reduced threshold voltage. *2017 29th International Symposium on Power Semiconductor Devices and IC's (ISPSD), Sapporo, Japan*; IEEE: 2017; pp 355−358. DOI: DOI: 10.23919/ISPSD.2017.7988991.
(23) Chou, S. Y.; Chang, Y.; Weiner, K. H.; Sigmon, T. W.; Parsons, J. D. Annealing of implantation damage and redistribution of impurities in SiC using a pulsed excimer laser. *Appl. Phys. Lett.* **1990**, *56*, 530−532.
(24) Ahmed, S.; Barbero, C. J.; Sigmon, T. W. Activation of ion implanted dopants in α-SiC. *Appl. Phys. Lett.* **1995**, *66*, 712−714.
(25) Hishida, Y.; Watanabe, M.; Nakashima, K.; Eryu, O. Excimer Laser Annealing of Ion-Implanted 6H-Silicon Carbide. *Mater. Sci. Forum* **2000**, *338*−*342*, 873−876.
(26) Tanaka, Y.; Tanoue, H.; Arai, K. Electrical activation of the ion-implanted phosphorus in 4H-SiC by excimer laser annealing. *J. Appl. Phys.* **2003**, *93*, 5934−5936.
(27) Schroder, D. K. *Semiconductor Material and Device Characterization*, 3rd ed.; John Wiley & Sons Inc.: Hoboken, NJ, USA, 2006.
(28) Sorieul, S.; Costantini, J.-M.; Gosmain, L.; Thomé, L.; Grob, J.-J. Raman spectroscopy study of heavy-ion-irradiated α-SiC. *J. Phys.: Condens. Matter.* **2006**, *18*, 5235−5251.
(29) Nakashima, S.; Mitani, T.; Tomobe, M.; Kato, T.; Okumura, H. Raman characterization of damaged layers of 4H-SiC induced by scratching. *AIP Adv.* **2016**, *6*, 015207.
(30) Zwick, A.; Carles, R. Multiple-order Raman scattering in crystalline and amorphous silicon. *Phys. Rev. B* **1993**, *48*, 6024−6032.
(31) Choi, I.; Jeong, H. Y.; Jung, D. Y.; Byun, M.; Choi, C.-G.; Hong, B. H.; Choi, S.-Y.; Lee, K. J. Laser-Induced Solid-Phase Doped Graphene. *ACS Nano* **2014**, *8*, 7671−7677.
(32) Ferrari, A. C.; Meyer, J. C.; Scardaci, V.; Casiraghi, C.; Lazzeri, M.; Mauri, F.; Piscane, S.; Jiang, D.; Novoselov, K. S.; Roth, S.; Geim, A. K. Raman Spectrum of Graphene and Graphene Layers. *Phys. Rev. Lett.* **2006**, *97*, 187401.
(33) Burton, J. C.; Sun, L.; Long, F. H.; Feng, Z. C.; Ferguson, I. T. First- and second-order Raman scattering from semi-insulating 4H-SiC. *Phys. Rev. B* **1999**, *59*, 7282−7284.
(34) Ferrari, A. C.; Robertson, J. Interpretation of Raman spectra of disordered and amorphous carbon. *Phys. Rev. B* **2000**, *61*, 14095−14107.
(35) Usman, M.; Nour, M.; Azarov, A. Y.; Hallén, A. Annealing of ion implanted 4H−SiC in the temperature range of 100−800 °C analysed by ion beam techniques. *Nucl. Instrum. Meth. Phys. Res. B* **2010**, *268*, 2083−2085.
(36) Mazzamuto, F.; Halty, S.; Mori, Y. Silicon Carbide Recrystallization Mechanism by Non-Equilibrium Melting Laser Anneal. *Mater. Sci. Forum* **2016**, *858*, 540−543.
(37) Lee, S.; Toney, M. F.; Ko, W.; Randel, J. C.; Jung, H. J.; Munakata, K.; Lu, J.; Geballe, T. H.; Beasley, M. R.; Sinclair, R.; Manoharan, H. C.; Salleo, A. Laser-Synthesized Epitaxial Graphene. *ACS Nano* **2010**, *4*, 7524−7530.
(38) Jeong, T.; Zhu, J.-G.; Mao, S.; Pan, T.; Tang, Y. J. Thermal Characterization of SiC Amorphous Thin Films. *Int. J. Thermophys.* **2012**, *33*, 1000−1012.
(39) Musumeci, P.; Reitano, R.; Calcagno, L.; Roccaforte, F.; Makhtari, A.; Grimaldi, M. G. Relaxation and crystallization of amorphous silicon carbide probed by optical measurements. *Philosophical Magazine B* **1997**, *76*, 323−333.
(40) Levinshtein, M. E.; Rumyantsev, S. L.; Shur, M. S. *Properties of Advanced Semiconductor Materials: GaN, AIN, InN, BN, SiC, SiGe*; John Wiley & Sons, 2001; p 137.
(41) Schroder, D. K. *Semiconductor Material and Device Characterization*, 3rd ed.; Wiley: New York, 2006.
(42) Spera, M.; Greco, G.; Corso, D.; Di Franco, S.; Severino, A.; Messina, A. A.; Giannazzo, F.; Roccaforte, F. Ohmic Contacts on p-Type Al-Implanted 4H-SiC Layers after Different Post-Implantation Annealings. *Materials* **2019**, *12*, 3468.

https://doi.org/10.1021/acsaelm.2c00748
ACS Appl. Electron. Mater. 2022, 4, 4514−4520